Experimental demonstration of realizability of optical focus wave modes

Kaido Reivelt and Peeter Saari
Institute of Physics, University of Tartu, Riia 142, 51014 Tartu, Estonia
(Received 31 July 2002; published 26 November 2002)

The homogeneous scalar wave equation has a number of so-called localized wave (LW) solutions, instantaneous, Gaussian pulselike intensity distribution of which propagates without any spread or distortions in free space. Despite the undoubtedly intriguing properties and considerable effort that has been made to implement such wave fields, in the optical domain only their limiting case—the so-called Bessel-*X* pulses—has been experimentally launched so far. In this paper we report on experimental evidence of the optical realizability of the ''fundamental'' special case of the LW's—the focus wave modes.

DOI: 10.1103/PhysRevE.66.056611 PACS number(s): 42.25.Bs, 42.15.Eq, 42.65.Re, 42.25.Kb

I. INTRODUCTION

During the last two decades it has been established that the homogeneous wave equation has a number of so-called localized wave (LW) solutions, instantaneous, Gaussian pulselike intensity distribution of which propagates without any spread or distortions in free space (see Ref. [1] for a general review, also Refs. [2–27], and references therein). In a theoretical limit, the spatial amplitude distribution of optical-domain LW solutions may consist of an intense central peak of micrometer diameter on a sparse low-intensity background that travels without any transversal and/or longitudinal spread in free space. In realizable optical systems, for finite-energy and finite-aperture wave fields, the depth of such an invariant propagation is finite, yet it considerably exceeds the length of the waist of common focused fields.

The spatial and temporal localization makes the implementation of LW solutions very attractive for applications where the lateral and (or) transversal diffractional spread of optical wave fields is a major limitation of the system performance (e.g., optical communication, metrology, monitoring, imaging, terahertz and femtosecond spectroscopy). However, it is only the launching of the limiting case, Bessel-*X* pulses, that has been accomplished in an optical experiment so far [14,15]. The ideas that have been proposed for generation of more complicated LW solutions (see, e.g., Refs. [1,4–7], and references therein) are hardly realizable in optical domain.

In our recent publications [16–18] we proposed an approach, how the complex optical LW solutions can be experimentally realized by making use of the wavelength dispersion of cone angle (axicon angle) of Bessel beam generators. In particular, we showed that good approximations to the fundamental LW solutions—focus wave modes (FWM's) [2,3,11,16]—can be generated by a combination of an axicon and a circular diffraction grating.

In this paper we present the experimental proof of the validity of this approach. As the first logical step we define a wave field that we call a two-dimensional FWM (2D FWM) and show that it shares all the characteristic properties of the FWM's. Also, we will show, that the optical generation of the two are in principle identical. Then we introduce our optical setup, designed for the generation of the 2D FWM's. The results of the experiments prove that our general idea of optical generation of FWM's [16] as well as the principles of our setup are valid and can be used to carry out further experiments in this field.

We start by presenting a short overview of the properties of the FWM's in Sec. II. Then, in Secs. III and IV, we give the general idea and the mathematical description of the experiment. In Sec. V we give the details of the setup. The results of the experiment and their discussion are presented in Sec. VI.

II. THE FUNDAMENTAL LOCALIZED WAVE SOLUTIONS—FOCUS WAVE MODES

The focus wave modes are the most widely known LW solutions of the scalar homogeneous wave equation. In terms of the angular spectrum of plane waves they can be described by the expression [11,16–18]

$$F(\rho,z,t)=\int_0^\infty dk\, a(k) J_0[k\rho \sin\theta_F(k)] \times \exp[ik\{z\cos\theta_F(k)-ct\}]. \quad (1)$$

Here $a(k)$ is the frequency spectrum of the wave field, $J_0(\,)$ is the zeroth-order Bessel function of the first kind and we have denoted

$$\theta_F(k)=\arccos\left[\frac{\gamma(k-2\beta)}{k}\right], \quad (2)$$

where γ and β are constants. Thus, the Eq. (1) can also be given the form

$$F(\rho,z,t)=\exp[-i2\beta\gamma z]\int_0^\infty dk\, a(k) J_0[k\rho \sin\theta_F(k)] \times \exp[ik(z\gamma-ct)]. \quad (3)$$

The expression (1) is essentially a cylindrically symmetric superposition of monochromatic Bessel beams $J_0[k\rho\sin\theta]\exp[ik(z\cos\theta-ct)]$ [19] and Eq. (2) determines the support of angular spectrum of plane waves of the wave field [see Fig. 1(a) for an example]. The constant γ determines the group velocity of the wave field as $v_g=c/\gamma$ and parameter 2β has an interpretation as being the wave num-

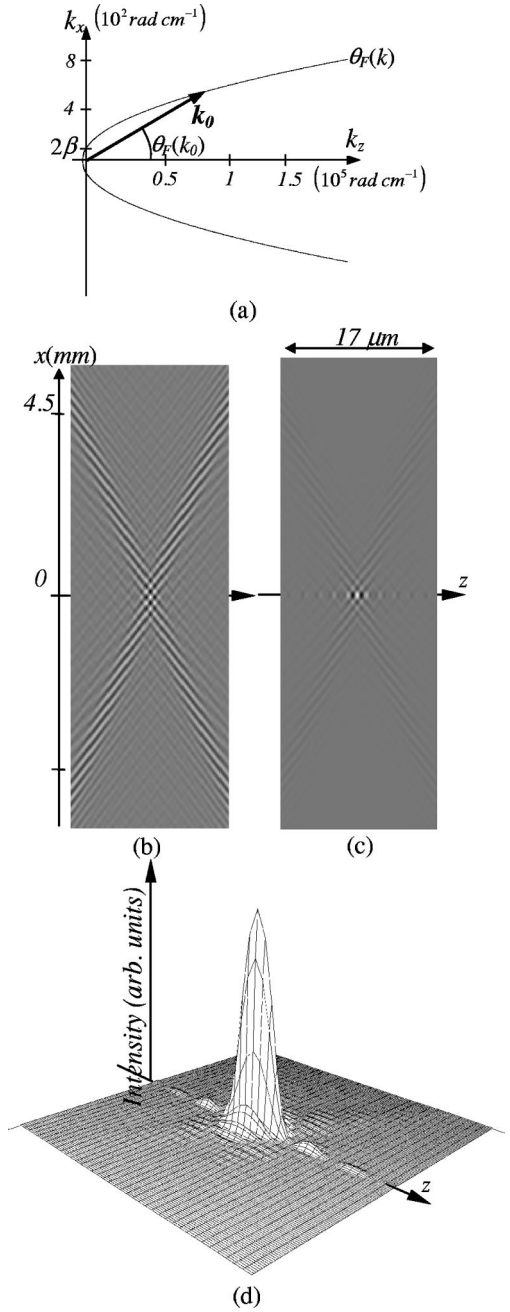

FIG. 1. On the general description of the FWM's and 2D FWM's. The examples here were calculated with the following protect $\beta=40$ rad/s, $\gamma=1$ giving $\theta_{FWM}(k_0)\sim 1.3°$ if $k_0=7.8\times 10^6$ rad/m ($\lambda_0\sim 800$ nm), the frequency spectrum $a(k)$ is uniform between the wavelengths 600 to 1000 nm: (a) the k_xk_z-plane section of the support of the angular spectrum of plane waves of the wave fields (note that for FWM's the support is of the cylindrical symmetry), (b) the spatial amplitude distribution of the 2D FWM in xz plane, (c) the spatial amplitude distribution of the FWM in xz plane, (d) the central part of the instantaneous intensity distribution of the FWM.

ber of the plane wave component of the angular spectrum that propagates perpendicularly to z axis [see Fig. 1(a)]. The FWM's have also been called ''fundamental'' LW solutions because they have been used to construct the more general classes of LW's [1,11]

The wave field (1) has been shown to possess the following properties [11,16–18].

(1) The wave field can be constructed so that its instantaneous intensity distribution has a narrow on-axis central peak of the diameter of few micrometers. The pulse's longitudinal profile is generally that of the corresponding transform-limited Gaussian pulse [see Figs. 1(c) and 1(d)].

(2) The spatial shape of the central peak does not change or spread, neither transversally nor longitudinally in the course of propagation in free space.

(3) Generally the on-axis phase velocity of the wave packet is different from its on-axis group velocity, the difference being determined by the constant β in Eq. (2). The effect is also known as the local variations of the central peak of the wave field (see Refs. [1,20], and references therein).

(4) The wave packets with different on-axis group velocities v^g can be constructed from Eqs. (1) and (2).

(5) The limiting case $\beta=0$ in Eq. (1) yields the simplest class of LW's—X pulses and Bessel-X pulses [21–27]. For them not only the instantaneous intensity distribution but also the field itself propagates without any change along the optical axis having equal phase and group velocities, both necessarily superluminal.

In our opinion the peculiar properties of the FWM's can be given physically the most transparent interpretation by treating them as the cylindrically symmetric superpositions of the interfering pairs of certain tilted pulses [20] (this approach has also been used to discuss the properties of X-type pulses, in this case the components of the interfering pair are the limiting case of the tilted pulses—plane wave pulses [14]). In this representation the spatial amplitude distribution of the FWM's can be expressed as

$$F(\rho,z,t)=\int_0^\pi d\phi[T(x,y,z,t;\phi)+T(x,y,z,t;\phi+\pi)]$$
$$\equiv\int_0^\pi d\phi F_{2D}(x,y,z,t;\phi), \tag{4}$$

where $T(x,y,z,t;\phi)$ is the spatial amplitude distribution of the tilted plane wave pulses, which in the spectral representation is given by

$$T(x,y,z,t;\phi)=\int_0^\infty dk\, a(k)\exp[ik\{x\cos\phi\sin\theta_F(k)+y\sin\phi\sin\theta_F(k)+z\cos\theta_F(k)-ct\}], \tag{5}$$

where the angular function $\theta_F(k)$ is defined by Eq. (2). From Eqs. (4) and (5) we get

$$F_{2D}(x,y,z,t;\phi)=\int_0^\infty dk\, a(k)\cos[k\sin\theta_F(k)(x\cos\phi+y\sin\phi)]\times\exp[ik\{z\cos\theta_F(k)-ct\}]. \tag{6}$$

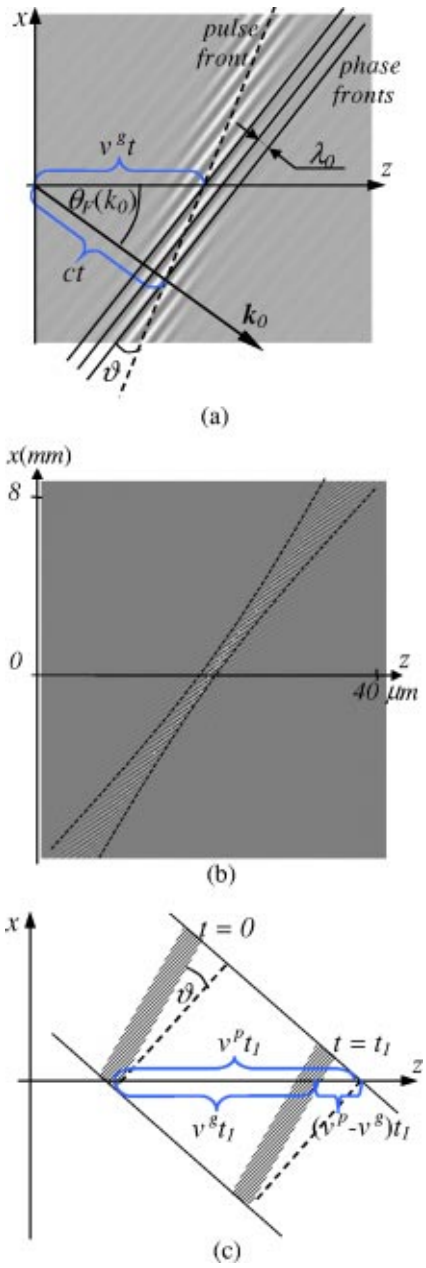

FIG. 2. On the properties of the tilted pulses: (a) an excerpt of the spatial amplitude distribution of a tilted pulse, here v_g and v_p denote group and phase velocities respectively, k_0 and λ_0 are the wave vector and the wavelength of the plane wave of the carrier wave number, t is an arbitrary time and ϑ is the tilt angle of the pulse, (b) the amplitude of the tilted pulse in larger scale, the dashed line marks the plane of equal intensity of the tilted pulse so that the ''waist'' of the tilted pulse can be clearly seen, (c) a geometrical illustration to the fact that the difference between the phase and group velocities of the tilted pulses is a direct consequence of the tilt between the phase fronts and the pulse front.

[An example of the spatial amplitude distribution of the tilted pulse in Eq. (5) is depicted in Fig. 2(a), the spatial amplitude distribution of the corresponding superposition of two tilted pulses in Eq. (6), and FWM's in Eq. (1) are depicted in Figs. 1(b) and 1(c), respectively.]

The representation (4) gives the properties of the FWM's the following interpretation:

(1) The localized central peak of FWM's is simply the well-known consequence of taking the axially symmetric superposition of a harmonic function (see Refs. [14,19] for example). Indeed, the interference of the two transform-limited tilted pulses in Eq. (6) gives rise to the harmonic interference pattern, the transversal width of which is proportional to the temporal length of the tilted pulses (5) and the central peak arises because in the superposition constructive interference occurs only on the optical axis. Formally, the cos() function in Eq. (6) is replaced by $J_0(\,)$ in Eq. (1) [compare Figs. 1(b) and 1(c)].

(2) The central peak does not spread because the support of the angular spectrum of plane waves of the tilted pulse (or FWM) is constructed so that the group velocity of the wide-band wave packet along the z axis is constant over the entire bandwidth [16–18]. Indeed, as

$$v^g = \left(\frac{dk_z}{d\omega}\right)^{-1}, \tag{7}$$

the Eq. (2) yields

$$k_z = k\cos\theta_F(k) = \gamma k - 2\beta\gamma \tag{8}$$

for the z-axis component of the wave vector, so that we get

$$v^g = \text{const} = c/\gamma. \tag{9}$$

The property can also be given a wave optical interpretation. Namely, it can be seen from Fig. 1(b), that the longitudinal length of the tilted pulses generally depends on the transversal coordinate and the tilted pulses have a ''waist.'' The relation (8) essentially guarantees that the waist propagates along the optical axis and does not spread—in this case the central peak of the corresponding cylindrically symmetric superpositions, FWM's (1), also remains transform-limited as it propagates.

(3) The difference of phase and group velocities along the optical axis is a direct consequence of the fact that the pulse and phase fronts of the tilted pulses are not parallel [20] (see Fig. 2, also Ref. [20] for the relevant discussion).

(4) The group velocity of the wave field can be set by changing the parameter γ in Eq. (2) or (8). Figure 2(b) gives the effect a clear physical interpretation—it can be seen, that the on-axis group velocity of the wave field in a simple geometric manner depends on the angle ϑ between the phase and pulse front (tilt angle), and also on the direction of the wave vector of the mean frequency. The free range of the parameters γ and β can be deduced by means of simple geometrical considerations. First of all, the angular spectrum of plane waves of the wave field should not contain any backward propagating plane waves components for which $k_z(k) > 0$ if we want the wave field to be causal for generation with a planar source. Also, as the propagation length of the central peak of the FWM is inversely proportional to the central cone angle $\theta_F(k_0)$ [16,19], the angular spectrum of plane waves of the wave field should subtend only paraxial

angles to the optical axis, i.e., the condition $\cos\theta_F(k)\sim 1$ should be satisfied in the entire spectral range of the wave field.

It is easy to see, that all the presented arguments are equally valid for the superpositions of tilted pulses in Eq. (6) and for its cylindrically symmetric counterparts—FWM's. Thus, we can state that the defined interfering pair of tilted pulses, inclined with respect to each other under the angle $2\theta_F(k_0)$, possesses all the characteristic properties of FWM's. This equivalence is also obvious if we compare the corresponding mathematical expressions (1) and (6)—the two are similar if we take $\phi=0$ and the polar coordinate ρ is understood as the transversal coordinate x in Eq. (6). In fact, the physics behind the two wave fields is similar to the degree, that we will call the wave field (6) as 2D FWM in what follows. Moreover, due to the more transparent physical interpretation, we will concentrate mostly on the 2D FWM's in present paper.

It is important to note that the exact form of the frequency spectrum $a(k)$ in Eqs. (1) and (6) is not restricted by any means. This is a direct consequence of the fact that the most important property of FWM's and 2D FWM's—their nonspreading propagation—is assured by the condition (2), i.e., by the *support* of the angular spectrum of plane waves of the wave fields [20]. Consequently, the spatial shape of the instantaneous intensity distribution of the FWM's (the presence of the sharp central peak, for example), determined also by the frequency spectrum $a(k)$ is not their most essential characteristic. Instead the FWM's should be described as wave fields that preserve their instantaneous intensity distribution, whatever it is. However, there is a common feature that can be attributed to all optically reasonable FWM's—the characteristic *X* branching [see Figs. 1(b) and 1(c)]. Though the transversal width and exact shape of the central, interfering part of the "*X*" depend on bandwidth and relative phases between the spectral components, its overall presence is encoded into the support of the angular spectrum of the plane waves.

It has to be emphasized that the representations (1) and (6) are not strictly physical in the sense that the total energy flow they contain is infinite. This inconvenience has been addressed in several works, mostly by deriving various finite energy flow approximations to FWM's that could also be launched from finite aperture (see Refs. [1,4–7], and references therein). In the context of present paper the most convenient approach is the one proposed in our recent publication Ref. [18]. In this paper we gave a simple mathematical description of the effect of finite aperture to the outcome of the optical setup implemented in present work and demonstrated that in such setups the finite aperture of the optical system automatically eliminates the infinite energy flow so that the generated wave field is strictly physical. In fact, the only qualitative effect the finite-energy approximation introduces is the finite propagation length of the wave fields. The results of this paper confirm the validity of this approach.

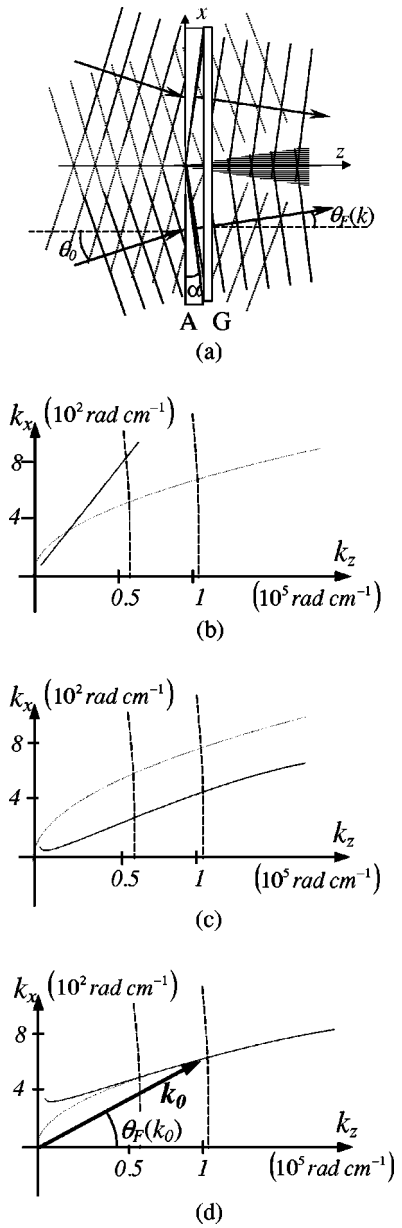

FIG. 3. (a) The FWM generator consist of an axicon *A* and of an circular diffractional grating G (or two wedges and linear diffractional grating, respectively, if we generate 2D FWM's), the FWM can be observed in the conical volume (striped region) behind the diffraction grating; (b) The support of the angular spectrum of plane waves of the initial wave field on the FWM generator (solid line). Here and hereafter the dotted line denotes the support of angular spectrum of plane waves of the (2D) FWM under discussion, the dashed lines denote the bands of the frequency spectrum of the light used in our experiments (note the difference in scales between k_x and k_z axis); (c) The support of the angular spectrum of plane waves behind the axicon; (d) The support of the angular spectrum of plane waves at the exit of the FWM generator as compared with the theory.

III. THE GENERAL IDEA OF OPTICAL GENERATION OF FWM'S

The general idea of optical generation of FWM's can be introduced as follows. Consider the pair of plane wave pulses propagating at angles θ_0 and $-\theta_0$ relative to the optical axis [see Fig. 3(a)]. Obviously we can introduce a tilt into the angular spectrum of plane waves by means of the angularly dispersive elements like diffraction gratings or

prisms (wedges). Provided that the resulting tilted pulses overlap, we can observe the interference of two tilted pulses in near-axis conical volume [see the striped region in Fig. 3(a)]. If the support of the spectrum of the plane wave components of the tilted pulses is the one described by the Eq. (2) and if we ignore for the while the diffractional edge effect that appears due to the finite aperture of the optical elements, the interference pattern in the near-axis volume is that of the 2D FWM's described by Eq. (6). Consequently, in this approximation the optical generation of 2D FWM's reduces to the modeling of a set of diffractive elements that transform the support of the angular spectrum of plane waves of the input wave field so that the angular dispersion of the output pulse approximates the one described by the condition in Eq. (2) and to the ''compression'' of the resulting wave field by compensating for the relative phases between its monochromatic components so that a transform-limited pulse appears on the optical axis. The former problem has been resolved in Ref. [16]—it has been shown that a good approximation to the tilt of the angular spectrum (2) can be generated by means of the combination of a prism and a diffraction grating. The latter task will be discussed later in present paper.

The cylindrically symmetric case in Eqs. (1) and (4) can be considered as a straightforward generalization of this approach. In this case the prism and diffraction grating are replaced by their circularly symmetric counterparts—axicon and a circular diffraction grating (see Ref. [16]). The cylindrically symmetric counterpart of the initial superposition of the two plane wave pulses (the Bessel-X pulse or X pulse [21,25–27]—can be generated by means of a combination of a circular slit and a Fourier lens [14].

In this paper we experimentally implement the former, essentially one-dimensional case of the general idea and optically implement 2D FWM's. We decided so mostly because the physical concept is much more clear in this sort of experiments. However, it also appeared that the fabrication and polishing of a high-quality, large aperture concave conical surface is still a complicated task.

IV. SETUP

The setup of our experiment is depicted in Fig. 4. The main part of it is the FWM generator (see grayed area in Fig. 4). The FWM generator is placed into an arm of an interferometer.

The FWM generator consists of the mirrors $M7$ and $M8$, the two wedges $W1$ and $W2$, and a blazed diffraction grating G. The Snell's law and the grating equation yield the following equation for the direction of propagation of the monochromatic plane wave component behind the elements [16]:

$$\sin\theta_G(k)=\frac{2\pi}{kd}+n(k)\sin\left[-\alpha+\arcsin\left(\frac{1}{n(k)}\sin(\theta_0+\alpha)\right)\right], \tag{10}$$

here α is the angle of the wedges, d is the groove spacing of the diffraction grating, θ_0 is the angle the initial plane wave pulse subtends to the optical axis, and $n(k)$ is the refractive index of the axicon and grating material (the sign conventions are chosen so that the angles $\alpha,\theta_0,\theta_G(k)$ are positive in Fig. 3(a), first-order diffraction is assumed).

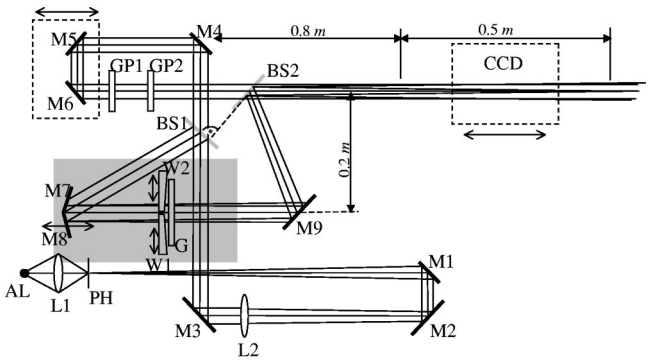

FIG. 4. Experimental setup for generating 2D FWM's and recording its interference with plane wave pulses. The FWM generator can be seen in grayed area; M's, mirrors; L's, lenses; BS's, beam splitters; W's, wedges; G, diffractional grating; AL, Xe-arc lamp; PH, pinhole.

In our experiment we implemented a 2D FWM with following parameters: $\beta=40$ rad/m, $\gamma=1$ giving $\theta_F(k_0)\sim 0.26°$ if $k_0=7.8\times10^6$ rad/m ($\lambda_0\sim800$ nm) [see Fig. 1(c) for the corresponding theoretical spatial amplitude distribution and Ref. [16]]. The optimization of the parameters α, θ_0, and d in Eq. (10) yields $\alpha=1.204\times10^{-2}$ rad, $d=3.749\times10^{-4}$ m and $\theta_0=9.468\times10^{-3}$ rad [see Figs. 3(b–d) for the transform of the support of the angular spectrum of plane waves introduced by the optical elements]. The comparison of the angular spectrum support, determined by Eq. (10) to the one of the FWM in Eq. (2) is depicted in Fig. 3(d).

We used interferometric cross-correlation methods with time-integrated intensity recording to study the generated wave field. The FWM generator has been placed in what is basically a specially designed, modified Mach-Zehnder interferometer. The interferometer consists of two beam splitters and identical broadband nondispersive mirrors. The input field from the light source is split by the beams plitter BS1 into the fields that travel through the two arms of the interferometer, the one with the FWM generator and the arm for the reference beam. The mirrors $M5$ and $M6$ form a delay line; they were translated by the Burleigh Inchworm linear step motor, the 1 μm translation step of which was reduced to 65 nm by a transmission mechanism. The mirror $M7$ was continuously translatable as to correct for the time shift between the two tilted pulses. The wedges $W1$ and $W2$ were transversally translatable so as to balance the material dispersion they introduce to the plane wave pulses (see text below). We used Kodak Megaplus 1.6i charge-coupled device (CCD) camera with the 1534×1024 matrix resolution and 10 bit pixel depth. The linear dimensions of the matrix are 13.8 mm$(H)\times$9.2 mm(V), the pixel size is 9 μm$\times$9 μm.

A very challenging part of the setup is the light source—computer simulations, or even simple geometrical estimations show that if the autocorrelation time of the source field τ exceeds $\sim$10 fsec, the characteristic X branching [see Figs. 1(b)and 1(c)] occurs too far from the axis z and in this narrow-band limit the resulting wave field would be nothing

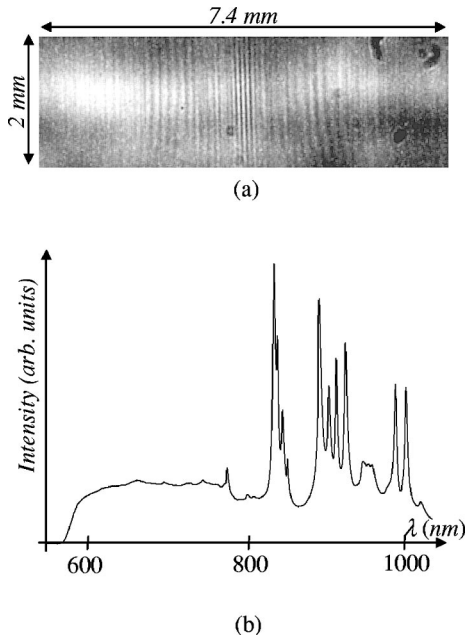

FIG. 5. (a) A typical interferogram in the setup as recorded by the CCD camera, (b) the power spectrum of the light used in our setup.

but a trivial interference of quasimonochromatic plane waves. However, as the cross-correlation measurement technique has been chosen, we do not need transform-limited femtosecond pulses as the input light field. Instead, we can use a source of a stationary white noise. This is the case, because the time-integrated mutual intensity recordings are insensitive to phase relations between different temporal Fourier's components of the field, i.e., the intensity recordings are sensitive only to the changes of relative phases of the temporal Fourier' components in the two arms of the interferometer (see Ref. [28] for example). In our experiment we used the filtered light form a superhigh pressure Xe-arc lamp, giving ~ 6 fsec correlation time for the input field [see Fig. 5(b) for the power spectrum of the light].

The well-known drawback of the choice is the hugely reduced signal level—to ensure good transversal coherence over the clear aperture of the setup the white light has to be spatially filtered by means of a pinhole (PH in Fig. 4). The required diameter ~ 15 μm of the pinhole and focal length 2 m of the collimating Fourier lens L1 was estimated from the van Cittert-Zernike theorem [29] for the mean wavelength of the light, $\lambda_0 = 800$ nm. As a result of the filtering, the total power of the signal on the ~ 1.5-cm^2 CCD chip was ≈ 0.03 μW.

Due to the short coherence time of the source field, the experiment is also highly sensitive to the phase distortions (spectral phase shift) introduced by the dispersive optical elements of the system—the beam splitters and the FWM generator. In the FWM generator there are three possible sources of undesirable dispersion: (1) the propagation in the glass substrate of the diffraction grating, (2) the propagation between the grating and the axicon where the support of angular spectrum of the wave field is not appropriate for the free space propagation, i.e., it does not obey Eq. (2), and (3) the propagation in the wedges. The beam splitters in our setup are identical and if we set them perpendicularly and orient the coated sides so that each beam passes the glass substrate of the beam splitter twice, the arms of the interferometer remain balanced. The influence of the propagation between the elements can be made negligible by placing them close to each other. The character of the undesirable dispersion in the wedges can be estimated from the following considerations. The entrance wave field on the wedges is the transform-limited Bessel-X pulse, so, the on-axis part of the pulse is also transform limited and should pass through the wedges unchanged, i.e., without any additional spectral phase shift. Consequently, the wedges should be produced and aligned so that their thickness is zero on the optical axis. As the apex angle of the wedges is very small in our setup ($\sim 0.7°$), this is not a very practical approach and we consider the finite thickness on the axis as the source of additional spectral phase shift instead. Thus, the composite spectral phase shift of the FWM generator can be described as the phase distortion introduced by the substrate of the diffraction grating and by a glass plate of the material of the wedges, the thickness of which is equal to the thickness of the wedges on the optical axis.

Apparently the introduced spectral phase shift can be eliminated by applying conjugate phase distortion to the initial field in the FWM generator arm of the interferometer and this can be done by means of the dispersion compensation techniques routinely used in femtosecond optics. However, we take a more straightforward approach and simply balance the arms of the interferometer by inserting material dispersion into the reference arm of the setup by means of two appropriate glass plates (GP1 and GP2 in Fig. 4).

In principle, the femtosecond pulses are also sensitive to the dispersion of the air and we should replace k_z by $k_z n(\omega)$ in Eqs. (7)–(9), $n(\omega)$ being the refractive index of the air. This modification yields the following equation for the support of the angular spectrum of plane waves of the FWM:

$$\theta_F\left(\frac{\omega}{c_0}\right) = \arccos\left[\frac{\gamma\left(\frac{\omega}{c_0} - 2\beta\right)}{n(\omega)\frac{\omega}{c_0}}\right], \tag{11}$$

where c_0 is the velocity of light in vacuum. In fact, Eq. (11) is of quite general interest, as it defines the support of angular spectrum of plane waves to the wave field that propagates without any longitudinal or transversal spread in linear dispersive media. This approach—to use predetermined angular dispersion to suppress the longitudinal (and transversal) dispersion—thought differently formulated, has been already used in Refs. [15,30,31]. However, in interferometric experiments we can use Eq. (2) instead of Eq. (11) as long as the arms of the interferometer are of equal length.

To finish this section we note the following. Obviously we should keep in mind that we are measuring interference patterns of the partially coherent wave fields, not of the transform-limited optical pulses. However, due to the known insensitivity of the interferometric experiments to the phase

relations between different temporal Fourier's components of the wave fields and for the convenience of the representation we will not call attention to this circumstance in what follows and, for brevity, use the terminology of the coherent, pulsed optical wave fields instead. In our forthcoming publication we will present the following discussion in the terms of second-order coherence theory.

V. MATHEMATICAL DESCRIPTION OF THE EXPERIMENT

In our experiment the superposition of the two tilted pulses—the 2D FWM—interferes with a plane wave pulse V_P,

$$V(\mathbf{r},t)=F_{2D}(\mathbf{r},t)+V_P(\mathbf{r},t). \tag{12}$$

Here

$$V_P(\mathbf{r},t)=\int_0^\infty dk\, a(k)b_P(k)\exp[ik\{z-c(t+\tau)\}], \tag{13}$$

$b_P(k)$ being the spectral phase shift introduced by the optics in the reference arm of the interferometer, $|b_P(k)|\equiv 1$, and τ denote the time delay between the two pulses. For the 2D FWM we have

$$F_{2D}(\mathbf{r},t) = \int_0^\infty dk\, a(k)b_F(k)\cos[kx\sin\theta_F(k)] \times\exp[ik\{z\cos\theta_F(k)-ct\}], \tag{14}$$

where $b_F(k)$ is the undesirable spectral phase shift from the 2D FWM generator, $|b_F(k)|\equiv 1$ (the nature of the phase functions $b_P(k)$ and $b_F(k)$ has been discussed in the preceeding section). The averaged intensity of the resulting wave field can be expressed as

$$\langle V^*V\rangle=\langle V_P^*V_P\rangle+\langle F_{2D}^*F_{2D}\rangle+2\ \mathrm{Re}\langle F_{2D}^*V_P\rangle, \tag{15}$$

where the angle brackets mean time average and we have omitted the arguments $(\mathbf{r},t)$ for brevity. The first term in the sum is the uniform intensity of the plane wave pulse,

$$\langle V_P^*V_P\rangle=\int_0^\infty dk\mathcal{A}(k), \tag{16}$$

$\mathcal{A}(k)=a^*(k)a(k)$ being the power spectrum of the wave field. The second term is the time-averaged intensity of the 2D FWM,

$$\langle F_{2D}^*F_{2D}\rangle=\int_0^\infty dk\mathcal{A}(k)\cos^2[kx\sin\theta_F(k)]. \tag{17}$$

For the third term we get

$$\langle F_{2D}^*V_P\rangle=\left\langle \int_0^\infty dk_1a^*(k_1)b_F^*(k_1)\cos[k_1\rho\sin\theta_F(k)] \times\exp[-ik_1\{z\cos\theta_F(k_1)-ct\}] \times\int_0^\infty dk_2a(k_2)b_P(k)\exp[ik_2\{z-c(t+\tau)\}]\right\rangle, \tag{18}$$

so that

$$\langle F_{2D}^*V_P\rangle=\int_0^\infty dk\mathcal{A}(k)b_F^*(k)b_P(k)\times\cos[k\rho\sin\theta_F(k)] \times\exp[-ikz\{\cos\theta_F(k)-1\}-ikc\tau]. \tag{19}$$

Assuming $\gamma=1$ and using Eq. (2) we get

$$\langle F_{2D}^*V_P\rangle=\exp[i2\beta z]\int_0^\infty dk\mathcal{A}(k)b_F^*(k)b_P(k) \times\cos[k\rho\sin\theta_F(k)]\exp[-ikc\tau]. \tag{20}$$

If the arms of the interferometer are balanced, the relation $b_F^*(k)b_P(k)\equiv 1$ holds and we have

$$\langle F_{2D}^*V_P\rangle=\exp[i2\beta z]\int_0^\infty dk\mathcal{A}(k)\times\cos[k\rho\sin\theta_F(k)] \times\exp[-ikc\tau]. \tag{21}$$

Equation (20) can also be given in the form

$$\langle F_{2D}^*V_P\rangle=\int_0^\infty dk\mathcal{A}(k)\cos[k\rho\sin\theta_F(k)] \times\exp[-ikz\cos\theta_F(k)+ikc(t_0-\tau)], \tag{22}$$

where $t_0=z/c$ and the constant has the interpretation of being the time that a wave field propagating at group velocity c travels the distance z to the plane of measurement. The integral expression (22) is very similar to the one describing the spatial amplitude distribution of the 2D FWM's Eq. (6), the only difference being that the frequency spectrum is replaced by the power spectrum $\mathcal{A}(k)$ in Eq. (22). Nevertheless, we cannot claim, that we actually detect the spatial amplitude distribution of the wave field under investigation (see also Ref. [14] for a relevant discussion). Indeed, as the absolute phases of the plane wave components are inevitably lost in interferometric experiments, we cannot say anything about the instantaneous amplitude distribution of the wave field. However, the interferograms *do* carry information about the *support* of the angular spectrum of plane waves—if the arms of the interferometer are balanced and the angular dispersion of the monochromatic plane wave components of the generated wave field is indeed as defined by Eq. (2), the interference patterns, described by Eq. (22), show the spatial amplitude distribution of the corresponding transform-limited wave field.

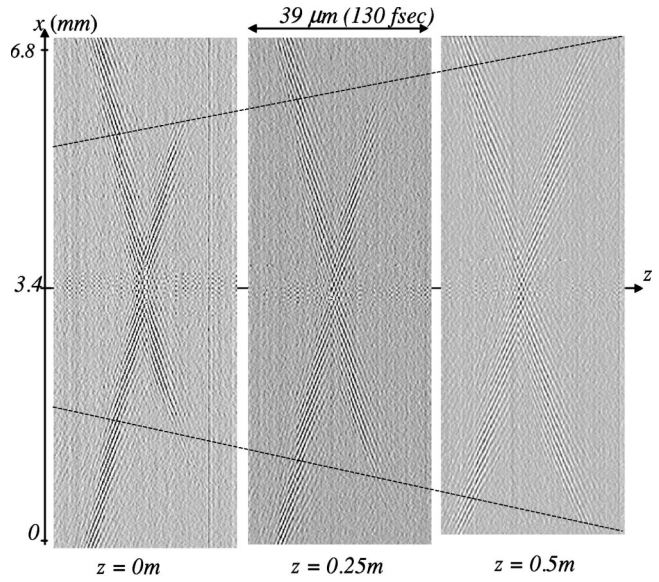

FIG. 6. The interference pattern in the setup as the function of the delay between the signal and reference wave fields in three positions of the CCD camera (see text for more detailed description).

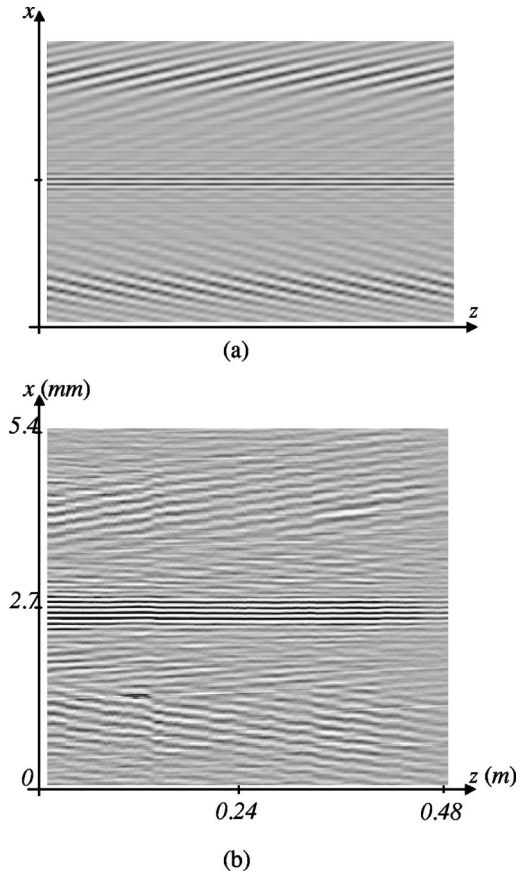

FIG. 7. The interference pattern as the function of the CCD camera position (see text for detailed description).

VI. THE EXPERIMENT

Our aim is to prove that the wave field generated in our setup shows all the characteristic properties of (2D) FWM's mentioned in the previous sections: the spatial amplitude distribution of the generated wave field (as defined in the end of the preceding section) should be transform limited and show the characteristic *X* branching in Fig. 1(b); it should propagate without transversal or longitudinal spread at the speed of the light in vacuum ($v^g = c$), its on-axis group and phase velocities should not be equal ($v^g \neq v^p$). To accomplish the task we use the direct correspondence between the description of the 2D FWM's in Eq. (6) and the description of interferograms in our experiment in Eq. (22).

In the first experiment we recorded the time-averaged interference pattern of the 2D FWM and the reference wave field as the function of the time delay between the two. The experiment can be mathematically modeled by varying parameter τ in Eqs. (15)–(21). We scanned the time delay at three *z*-axis positions, $z = 0$ cm, $z = 25$ cm, $z = 50$ cm (the origin of the *z* axis is about 30 cm away from the beam splitter BS2 in Fig. 4). In each experiment we recorded 300 interferograms, the time-delay step was 0.43 fsec (0.13 μm).

In a typical interference pattern in our experiment [see Fig. 5(a)] the sharp vertical interference fringes in the center correspond to the second term in the interference sum (15)—this is the ''propagation-invariant'' time-averaged intensity of the 2D FWM. The fringes can also be interpreted as the autocorrelation function of the interfering tilted pulses [see Fig. 5(b) for the corresponding power spectrum]. In this experiment the intensity of the wave field under study does not carry any important information, so we subtracted it numerically from the results in Fig. 6. The interference fringes that are symmetrically at both sides of the central part correspond to the third most important term in this sum. It can be seen from Fig. 5(a), that due to the low signal level the recorded interferograms are quite noisy. To get the better signal-to-noise ratio, we took the advantage of the known symmetry of the experiment and summed each interferogram vertically up and used the resulting one-dimensional data arrays instead.

The results of the experiment are depicted in Fig. 6. We can see that there is a good qualitative resemblance between the measured $x\tau$ plot of the interference pattern and the theoretical amplitude distribution of the 2D FWM's in Fig. 1(b). In Fig. 6 one can clearly see the characteristic *X* branching and the two interfering tilted pulses can be clearly recognized in the picture. Also, the wave field is definitely transform-limited, so we have managed to compensate for the spectral phase shift of the 2D FWM generator.

We can also see that the interference patterns do not show up any spread over the 0.5 m distance, consequently, the wave fields do not spread in the course of propagation.

An additional detail can be found in Fig. 6: the tilted pulses do not extend across the whole picture but are cut out (see dashed lines in Fig. 6). Also, the ''edges'' of the tilted pulses move away from the optical axis. This effect can be clearly interpreted as the consequence of the finite extent of the tilted pulses, as illustrated in Fig. 3(a) [20]—the dashed lines simply mark the borders of the volume, where the two tilted pulses intersect, i.e., the borders of the volume, where the 2D FWM exists [see the striped area in Fig. 3(a)].

In the second experiment we recorded the interference pattern as the function of the propagation distance z. The experiment can be simulated by varying z coordinate in Eq. (21). We recorded 240 interferograms, the step of the CCD camera position was 3.1 mm. The numerical simulation of the experiment together with the results of the experiment are depicted in Figs. 7(a) and 7(b), respectively.

The experiment can be easily interpreted—as the generated wave field is propagation-invariant, the position-invariant envelope of the interference pattern is the consequence of the fact that the group velocity of the 2D FWM is c (the reference plane wave pulse propagates with this velocity). The z-dependent finer structure of the interferograms is the consequence of the fact that the phase velocities of the plane wave pulse and 2D FWM are not equal, i.e., we have also $v^g \neq v^p$ for the phase and group velocities of the 2D FWM (see also Ref. [20]). The result of the experiment in Fig. 7(a) shows a good qualitative agreement with the theory.

We can also determine the parameter β from our experiment—the exponent multiplier in Eq. (21) reads $\exp[i2\beta z]$, thus $\beta = \pi / z_0$, where z_0 is the period of the variations along the z axis. From the result in Fig. 7(a) we estimated $z_0 \approx 7.5$ cm, so that $\beta \approx 42$ rad/m, which is in good agreement with the theory.

Thus, we have shown that the generated wave field has all the characteristic properties described in the previous theoretical sections and the validity of the general idea has been given an experimental proof.

VII. CONCLUSIONS

In this paper we presented the experimental evidence of the optical realizability of the fundamental LW solutions—focus wave modes. We constructed an optical setup for generation of two-dimensional FWM's and obtained results from interferometric measurements of the generated wave field that exhibits all the characteristic properties of the FWM's. Hence, our general idea of optical generation of FWM's [16], as well as the principles of our setup are valid and can be used to carry out more advanced experiments in this field.

ACKNOWLEDGMENT

This research was supported by the Estonian Science Foundation.

[1] I. Besieris, M. Abdel-Rahman, A. Shaarawi, and A. Chatzipetros, Prog. Electromagn. Res. **19**, 1 (1998).
[2] J.N. Brittingham, J. Appl. Phys. **54**, 1179 (1983).
[3] R.W. Ziolkowski, J. Math. Phys. **26**, 861 (1985).
[4] R.W. Ziolkowski, Phys. Rev. A **39**, 2005 (1989).
[5] P.L. Overfelt, J. Opt. Soc. Am. A **16**, 2239 (1999).
[6] A.M. Shaarawi, J. Opt. Soc. Am. A **14**, 1804 (1997).
[7] A.M. Shaarawi, I.M. Besieris, R.W. Ziolkowski, and S.M. Sedky, J. Opt. Soc. Am. A **12**, 1954 (1995).
[8] P.L. Overfelt, Phys. Rev. A **44**, 3941 (1991).
[9] R. Donnelly and R.W. Ziolkowski, Proc. R. Soc. London, Ser. A **440**, 541 (1993).
[10] R. Donnelly and R.W. Ziolkowski, Proc. R. Soc. London, Ser. A **437**, 673 (1992).
[11] A.M. Shaarawi, R.W. Ziolkowski, and I.M. Besieris, J. Math. Phys. **36**, 5565 (1995).
[12] P. Saari, Opt. Express **8**, 590 (2001).
[13] J. Salo and M.M. Salomaa, Pure Appl. Opt. **3**, 366 (2001).
[14] P. Saari and K. Reivelt, Phys. Rev. Lett. **79**, 4135 (1997).
[15] H. Sõnajalg, M. Rätsep, and P. Saari, Opt. Lett. **22**, 310 (1997).
[16] K. Reivelt and P. Saari, J. Opt. Soc. Am. A **17**, 1785 (2000).
[17] K. Reivelt and P. Saari, J. Opt. Soc. Am. A **18**, 2026 (2001).
[18] K. Reivelt and P. Saari, Phys. Rev. E **65**, 046622 (2002).
[19] J. Durnin, J.J. Miceli, Jr., and J.H. Eberly, Phys. Rev. Lett. **58**, 1499 (1987).
[20] K. Reivelt, Opt. Express **10**, 360 (2002).
[21] J. Lu and J.G. Greenleaf, IEEE Trans. Ultrason. Ferroelectr. Freq. Control **39**, 19 (1992).
[22] D. Mugnai, A. Ranfagni, and R. Ruggeri, Phys. Rev. Lett. **84**, 4830 (2000).
[23] E. Recami, Physica A **252**, 586 (1998).
[24] J. Lu and S. He, Opt. Commun. **161**, 187 (1999).
[25] P. Saari and H. Sõnajalg, Laser Phys. **7**, 32 (1997).
[26] P. Saari, in *Time's Arrows, Quantum Measurement and Superluminal Behavior*, Scientific Monographs: Physics Sciences Series (Italian CNR, Rome, 2001), p. 37; see Los Alamos archive http://xxx.lanl.gov/abs/physics/0103054.
[27] J. Fagerholm, A.T. Friberg, J. Huttunen, D.P. Morgan, and M.M. Salomaa, Phys. Rev. E **54**, 4347 (1996).
[28] K.B. Hill, S.A. Basinger, R.A. Stack, and D.J. Brady, Appl. Opt. **36**, 3948 (1997).
[29] L. Mandel and E. Wolf, *Optical Coherence and Quantum Optics* (Cambridge University Press, Cambridge, England, 1995).
[30] H. Sõnajalg and P. Saari, Opt. Lett. **21**, 1162 (1996).
[31] S. Szatmári, P. Simon, and M. Feuerhake, Opt. Lett. **15**, 1156 (1996).